Single-cell transcriptomics of the Arabidopsis floral abscission zone

Isaiah W. Taylor, O. Rahul Patharkar, Che-Wei Hsu, John Baer, Chad E. Niederhuth, Uwe Ohler, Philip N. Benfey*, John C. Walker*

*corresponding authors

Philip N. Benfey: philip.benfey@duke.edu

John C. Walker: walkerj@missouri.edu

Abstract

Abscission is the programmed separation of plant organs. It is widespread in the plant kingdom with important functions in development and environmental response. In Arabidopsis, abscission of floral organs (sepals, petals, and stamen) is controlled by two related receptor-like protein kinases HAESA/HAE and HAESA LIKE-2/HSL2, which are thought to orchestrate the programmed dissolution of the pectin-rich middle lamella between cells in the abscission zone, as well as the remodeling of the cell wall that occurs during abscission. Here, we report transcriptional characterization of the abscission zones of WT and the abscission deficient *hae hsl2* double mutant at single-cell resolution. We identify core abscission gene expression programs, as well as perturbations of differentiation dynamics in *hae hsl2*, including detecting expression changes in distinct spatial domains of the abscission zone. We also report identification of a novel negative regulator of abscission signaling, *MAP KINASE PHOSPHATASE-1/MKP1.* Mutating *MKP1* partially suppresses the abscission defect of *hae hsl2*. We establish the molecular basis of the suppression as reactivation of the *HAE/HSL2* pathway. Our results provide deep insight into the biology of abscission and establish it as a model developmental signaling system for interrogation by single-cell technologies.

Introduction

Abscission is a ubiquitous process occurring at multiple stages of the plant life cycle. Shedding of leaves in the autumn and fruit after ripening are common examples, as is shedding of organs after damage or infection[1–3]. Historically, selection for grass varieties with defects in seed abscission (also known as shattering) dramatically increased the efficiency of harvest and is considered one of the critical steps in domestication[4]. Controlling abscission today is still of agricultural and horticultural relevance. A number of crops including citrus, cotton, brassica, and some rice varieties suffer yield loss due to abscission[5–8].

The study of abscission dates back to at least the 19th century with detailed anatomical analyses[1]. Mid-20th century physiologists used leaf abscission as a model to begin to define molecular regulation of the process, establishing that interaction of the hormones ethylene and auxin regulate abscission in a number of species[1]. In the genomics era, abscission of tomato pedicels and Arabidopsis floral organs are among the best studied systems[9,10]. In particular, Arabidopsis floral abscission has been shown to be regulated by ethylene, auxin, and their interaction[11–13], with additional contributions from jasmonic acid signaling[14]. In Arabidopsis, the site of floral abscission, known as the abscission zone (AZ), is lignified on the distal margin to create a well-defined separation plane[15]. During abscission, the middle lamella (the pectin-rich interstitial substance adhering adjacent cells) is degraded enzymatically before the organs detach[16].

Abscission in Arabidopsis is regulated by two related leucine-rich repeat receptor-like protein kinases (LRR-RLKs) HAESA/HAE and HAESA LIKE-2/HSL2. The double mutant *hae hsl2* fails to shed its floral organs [Figure 1A] [17–19]. Several major components of the *HAE/HSL2* signaling pathway regulating abscission have been discovered [Figure 1B]. In particular, HAE and HSL2 cooperate with members of the SOMATIC EMBRYOGENSIS RECEPTOR KINASE/SERK family of co-receptor LRR-RLKs to bind the secreted INFLORESCENCE DEFICIENT IN ABSCISSION/IDA peptide, which activates a MAP kinase cascade comprised of MAP KINASE KINASE-4 and -5(MKK4/5) and MAP KINASE-3 and -6 (MPK3/6). One validated target of this MAPK cascade is the transcription factor AGL15, which is phosphorylated in a MAPK-dependent manner and negatively regulates *HAE* expression, forming a component of a positive feedback loop[20]. MAPK signaling also triggers expression of downstream abscission genes involved in pectin degradation, cell wall remodeling, and, ultimately, separation of the abscising organs[18,21–25], in a process presumably regulated by activation of additional unidentified transcription factors. In addition, the spatial pattern of expression of the *IDA* gene has been shown to be controlled by ethylene, providing a molecular link between IDA-HAE/HSL2 signaling and hormonal regulation of floral abscission[26].

Arabidopsis floral development has been described in stages[27,28]. By stage 15, pollination has occurred and the silique has elongated just beyond the petals [Figure 1C]. At stage 16, the silique continues to elongate while floral organs have withered and are nearing abscission. Stage 17 is a long post-abscission period during which the silique completes elongation. We have previously shown a *HAEpr::HAE-YFP* transgene can rescue the loss of abscission defect of a *hae hsl2* mutant, and that expression of *HAE* increases dramatically in the AZ at stage 15 [Fig. 1D][20,29]. An experimental approach that has proven useful in identifying genes associated with abscission involves manually dissecting the base of the flower (called the receptacle) of stage 15 flowers of both WT and *hae hsl2* (at which point major morphological changes have not yet occurred) and performing transcriptomic comparisons [e.g. [25,30]]. These experiments indicate that by stage 15, *HAE/HSL2* signaling has been activated to regulate the expression of a core set of genes primarily involved in pectin degradation and cell wall remodeling.

A limitation of these analyses is that the vast majority of cells in the receptacle are not in the AZ, and only a limited number of genes are known *a priori* to be specific to the AZ[11]. Therefore, it is plausible that some of the observed gene expression changes are secondary effects of *HAE/HSL2* signaling, occurring elsewhere in non-AZ cells. In addition, there may be some genuinely differentially expressed genes in the AZ missed in bulk analyses due to dilution of signal from inclusion of non-AZ cells. Alternative isolation approaches such as laser capture microdissection of fixed tissue and bulk RNA-Seq of sorted AZ cells have been employed and are informative[15,31]. However, these techniques fail to capture global patterns of gene expression both in and outside of the AZ, can be labor intensive, and offer limited fine-grained expression information.

To address these shortcomings, we used single-cell RNA-Sequencing (scRNA-Seq) to compare WT and *hae hsl2*, performing replicated experiments on floral receptacle derived protoplasts. We supplemented floral receptacle data with replicated scRNA-Seq on FACS sorted cells expressing either functional HAE-YFP or kinase dead HAE-YFP K711E (mutated at the conserved catalytic lysine K711). The expression of both constructs is highly enriched in the AZ, but kinase-dead HAE-YFP K711E does not complement the mutant phenotype [Figure 1E]. This experimental system is summarized in Figure 1F. The resulting dataset allowed us to robustly identify AZ cells, which we validated through multiple approaches. Differential expression analysis between WT and *hae hsl2* identified a large number of genes involved in pectin degradation, cell wall remodeling, and extracellular barrier formation (cutin/lignin). We provide

evidence that single-cell analysis of stage 15 AZs captures differentiating cell populations reflecting the spatial organization of the AZ, identifying proximal AZ cells (those retained on the plant) and distal AZ cells (those at the base of the abscising organs). We further show that the *HAE/HSL2* pathway promotes this differentiation process. Finally, we identify a core set of validated *HAE/HSL2* regulated AZ genes identifiable by bulk RNA-Seq. We demonstrate the utility of this robust expression signature by characterizing newly identified suppressors of *hae hsl2* mutated in the *MAP KINASE PHOSPHATASE-1/MKP1* gene. Overall, this study establishes scRNA-Seq as an insightful approach to monitor the developmental signaling processes occurring during floral abscission.

Results

Single-cell RNA-Sequencing identifies floral abscission zone cells

We performed scRNA-Seq (2 replicates each) on stage 15 floral receptacles of WT and *hae hsl2*. We also profiled replicated samples of FACS sorted cells derived from *hae hsl2* expressing *HAEpr::HAE-YFP* (complementing) and kinase dead *HAEpr::HAE-K711E-YFP* (non-complementing) lines to enrich for both WT and mutant AZ cells (Materials and Methods). In total, we obtained data for 4 WT and 4 mutant replicate samples. After identifying putative multiplets and filtering low quality cells, we integrated all cells using Seurat[32], excluding genes whose expression was altered in a separate receptacle protoplast bulk RNA-Seq experiment (Materials and Methods). We used Louvain clustering to identify transcriptionally similar groups of cells and embedded them in a 2-dimensional Uniform Manifold Approximation and Projection (UMAP) [Figure 2A, top panel]. Next, we plotted WT cells on the UMAP expressing known markers of the AZ: *HAE* and the pectin degrading enzyme-encoding genes *QUARTET2/QRT2* and *POLYGALACTURONASE ABSCISSION ZONE OF A. THALIANA/PGAZAT* [Figure 2A, bottom panel]. A compact group of cells ("cluster 11") was apparent in the UMAP expressing all three AZ markers. These cells, numbering 869 out of a total of 16169 profiled WT cells (5.4%), grouped together across a wide range of Louvain clustering resolutions [Figure 2A, pink border, Supplemental Figure 1]. Thus, cluster 11 appears to represent the AZ, which is transcriptionally identifiable and highly distinct from other cell types in the receptacle.

To verify the identity of cluster 11, we took several approaches. First, we sorted *HAE-YFP* expressing cells and generated and sequenced bulk RNA-Seq libraries (Materials and Methods, Supplemental Table 1). We then calculated cluster-wise Spearman correlation between this dataset and "pseudo-bulk" data of each of the identified clusters from the single-cell experiment. Pseudo-bulking is a common analytical technique in single-cell analysis in which expression data for all cells of a particular type are summed into a single expression vector. Pseudo-bulk correlation analysis therefore provides a genome-wide measure of similarity between bulk data derived from sorted *HAE* positive cells and each cluster identified in the single-cell data. As expected, cluster 11 displayed the highest correlation, consistent with the hypothesis that it represents the AZ [Figure 2B, top panel]. Similarly, we took published bulk RNA-Seq data from sorted *QRT2*-expressing stage 16 AZ cells and performed an identical correlation analysis and found that, again, cluster 11 displayed the highest correlation [Figure 2B, bottom panel, Supplemental Tables 2 and 3][15]. Next, we identified four cluster 11 enriched genes not previously known to be specific to the AZ and generated promoter::fluorescent reporter lines [Figure 2C]. All four reporters displayed highly specific expression in the AZ cells, indicating cluster 11 represents the AZ.

While not the focus of this study, we were also curious if we could identify other non-AZ cell types present in the receptacle. Indeed, many genes associated with specific cell types from Arabidopsis leaf scRNA-Seq data were present in restricted clusters in our data[33], allowing us to make tentative assignments of epidermis, mesophyll, guard cells, etc [Supplemental Figure 2A-C]. This suggests that floral organs, as modified leaves, retain some of the gene expression patterns of their homologous organs. There were also clusters that did not express known leaf markers [Supplemental Figure 2B], likely representing less characterized, flower-specific cell types. For example, we identified a large group of cells expressing AT3G01420, an alpha dioxygenase encoding-gene previously shown to be highly enriched in bulk RNA-Seq of developing siliques[34], suggesting that there are uncharacterized flower-specific cell types [Supplemental Figure 2D].

The abscission zone expresses genes related to pectin degradation, cell wall remodeling, and extracellular barrier formation

To explore the biology of the putative AZ, we identified AZ enriched genes using Seurat (Materials and Methods, Supplemental Tables 4 and 5). Analysis of Gene Ontology (GO) terms found enrichment of genes associated with middle lamella degradation and cell wall remodeling (pectin catabolic process, polysaccharide catabolic process, galacturonan metabolic process, etc.) [Figure 2D]. Additionally, there were terms associated with extracellular barrier formation such as phenylpropanoid biosynthesis, the major pathway leading to lignin formation, which has been shown to play an important role in the delineation of the AZ in both Arabidopsis and rice[15,35]. Terms related to Fatty-acyl-CoA metabolism are associated with genes involved in cutin biosynthesis, a waxy substance deposited on the scar of newly differentiated epidermal cells after abscission has occurred[15]. Overall, these terms are highly consistent the AZ being a site of focused cell wall disassembly and barrier formation.

The *hae hsl2* mutant exhibits a reduction in expression of genes associated with core abscission zone signatures

We next examined the scRNA-Seq data to identify gene expression differences between *hae hsl2* and WT. Plotting mutant cells by UMAP indicates a similar spectrum of cell types as WT [Figure 3A], with a similar proportion of putative abscission zone cells numbering 964 out of 24497 profiled mutant cells (3.9%). To identify differentially expressed genes (DEGs), we performed pseudo-bulk analysis comparing WT to *hae hsl2* using edgeR[36]. This analysis revealed 302 genes with lower expression and 274 with higher expression in the double mutant as compared to WT [Supplemental Table 6].

GO term enrichment of genes with reduced expression in *hae hsl2* AZ was consistent with known biology of abscission, including terms related to pectin degradation and cell wall remodeling [Figure 3B, Materials and Methods]. Terms associated with suberin deposition are likely to reflect biosynthesis of cutin, a related wax compound with similar biosynthesis, which has been shown to accumulate in Arabidopsis floral AZs[15]. For visualization, we plotted the expression levels of a number of known and novel *HAE/HSL2* regulated genes [Figure 3C]. Overall, these results are consistent with the role of *HAE/HSL2* as central regulators of genes required for breakdown and remodeling of the cell wall during abscission. Interestingly, GO term analysis of genes with higher expression in *hae hsl2* did not reveal such clearly biologically interpretable signals and was enriched in terms associated with defense and hypoxia responses [Supplemental Figure 3]. This suggests there may be novel molecular pathways repressed by *HAE/HSL2* that can be interrogated in future work.

Single-cell RNA-Seq identifies spatial domains of the abscission zone

A recent report provided a detailed examination of the spatial organization of the AZ, identifying a differentiated group of cells on the distal side at the base of the abscising organ (termed *secession cells*) and a distinct group on the proximal side of the abscising organ (termed *residuum cells*) [Figure 4A][15]. Functionally, secession cells form a lignin "brace," which is thought to both focus the enzymatic activity of secreted hydrolases to the middle lamella of the fracture plane at the site of abscission, while also creating a rigid frame which "chips off" once sufficient weakening of the fracture plane has occurred. Conversely, the residuum transdifferentiates into epidermal cells exhibiting a protective cuticle layer.

This process had previously been detailed in stage 16 flowers, as abscission is occurring[15]. We hypothesized we may be able to detect evidence of the differentiation process at stage 15 from our data. Interestingly, when performing low resolution Louvain clustering of only WT AZ cells and embedding in UMAP space, two groups of cells emerge [Figure 4B, left panel]. We tested the hypothesis that these cells represent secession and residuum cells by performing cluster-wise Spearman correlation analysis with previously published bulk RNA-Seq data derived from sorted secession cells and, separately, sorted residuum cells[15]. Consistent with our hypothesis, we observed a strong association of one of the two clusters of cells with secession bulk data [figure 4B, middle panel] and strong association of the second group of cells with residuum bulk data [Figure 4B, right panel]. In addition, we found enrichment of a number of genes in the putative secession side associated with lignin biosynthesis such as the tandemly duplicated peroxidase genes *AT4G37520/AT4G37530* [Supplemental Figure 4A]. On the putative residuum side, we found enrichment of cuticle forming genes such as *ECERIFERUM3/CER3* and *PERMEABLE CUTICLE1/PEC1* [Supplemental Figure 4B].

HAE/HSL2 promote differentiation of residuum and secession cells

We next hypothesized that the *HAE/HSL2* pathway promotes specification of cellular identity of both secession and residuum cells. To test this hypothesis, we performed low-resolution Louvain clustering, secession and residuum correlation analysis, and UMAP embedding of mutant cells [Figure 4C, left panel]. While UMAP is a non-linear dimensionality reduction technique that inexactly represents true underlying variation, it is interesting that the UMAP embedding of the mutant cells is much less separated than that of WT. While the two clusters do indeed exhibit complementary correlation with secession and residuum cells [Figure 4C, middle and right panels], the degree of difference was much less than in WT. Taken together, these results suggest that in *hae hsl2,* the secession and residuum cells are not as transcriptionally differentiated as in WT. To test this hypothesis, we performed an analysis with edgeR to measure enrichment of genes in one group of cells or the other (Materials and Methods). In WT, we found a total of 846 out of a total of 23974 expressed genes which differed between the two cell types (Figure 4D, Supplemental Table 7). Using the same criteria in the mutant, we found a significantly fewer number of only 374 out of 22391 expressed genes differing (Figure 4D, Supplemental Table 8, p-value < 2.2e-16, Fisher's Exact Test). This is consistent with the hypothesis that the *HAE/HSL2* pathway promotes differentiation of both the secession and residuum sides of the AZ.

IDA expression is highly enriched in secession cells

Interestingly, while *HAE* is strongly expressed in both secession and residuum cells [Figure 4E], the *IDA* gene, encoding the secreted ligand of HAE, is the single most strongly enriched gene in secession cells [Figure 4F, Supplemental Table 7]. This pattern of *IDA* expression is consistent with both published

promoter::reporter and sorted bulk RNA-Seq experiments[15]. This suggests an elegant negative regulatory mechanism by which *IDA-HAE* signaling is activated and attenuated over the course of the abscission process. In this model, we propose soluble IDA peptide is initially secreted by secession cells and diffuses across the secession-residuum boundary to activate signaling in both cell types. However, once cell separation occurs, the source of the activating ligand (the abscising organ) is physically detached from the plant, leading to signal attenuation.

GO term enrichment analysis of secession and residuum cells suggests differing biological function

We were next interested to interrogate the differing biology of the putative secession and residuum cells. GO term enrichment analysis of secession cell-associated genes in wild type revealed modest enrichment of pathways related to phenylpropanoid biosynthesis [Figure 4G]. Since one of the main functions of the phenylpropanoid pathway is lignin formation, this is consistent with the idea that secession cells are in the early stages of forming a lignin brace. In contrast, genes associated with wild-type putative residuum cells are enriched in terms related to cellular activity such as protein production [Figure 4H]. This is consistent with classical observations that AZ cells are sites of high levels of protein synthesis[37].

Single-cell RNA-Sequencing and bulk RNA-Seq identify a partially overlapping set of DEGs between wild type and *hae hsl2*

Overall, these results indicate we can recover relevant biological processes and identify and validate changes in gene expression at the cell-type level in a single analysis. However, a major limiting factor for single-cell RNA-Seq analysis for routine transcriptional profiling is its expense. Therefore, an optimal research strategy may be to combine single-cell analysis with bulk RNA-Seq, which is considerably cheaper, for higher throughput transcriptomics focusing analysis on genes known to change specifically in a cell type of interest. To explore this possibility, we identified genes expressed at lower levels in *hae hsl2* both by scRNA-Seq and by previously published bulk datasets[Supplemental Table 9][24,30]. From this analysis we identified 67 genes [Supplemental Table 10], which were enriched in abscission-associated gene classes such as those related to pectin modification, fatty acid biosynthesis, and phenylpropanoid biosynthesis [Supplemental Figure 5]. This confirms bulk RNA-Seq is capable of detecting relevant changes in gene expression even in a small sub-population of cells such as the AZ in a sample of receptacle tissue.

***hae hsl2* suppressor mutants partially restore the abscission zone gene expression signature**

To validate the utility of this core set of *HAE/HSL2* regulated genes, we conducted a series of experiments on two unpublished *hae hsl2* suppressor mutants isolated from a previously described *hae hsl2* T-DNA suppressor screen[24]. These mutants, which we named *fal-3* and *fal-7* for *facilitated abscission locus,* display weak reduction in adhesion of the floral organs in plants grown in standard conditions at 22° [Fig 5A, left panels]. However, suppression of the *hae hsl2* phenotype was significantly increased when plants were grown at 16° [Figure 5A, right panels]. This can be quantified by measuring the force required to remove petals of stage 16 flowers [Fig 5B]. At 23°, there is a small but significant reduction in the force required to remove the petals as compared to *hae hsl2*. At 16° there is an approximately further 40% reduction in breakstrength, which is likely an underestimate of the effect since at 23° the breakstrength remains somewhat constant after stage 16, but at 16°, by stage 17, the breakstrength is often unmeasureable because the floral organs have abscised.

Based on the phenotypes, we hypothesized that the gene expression changes in *hae hsl2* would be partially reversed in the *hae hsl2 fal-3* and *hae hsl2 fal-7* suppressors. To test this hypothesis, we performed stage 15 receptacle bulk RNA-seq of plants grown at 16° comparing WT, *hae hsl2*, *hae hsl2 fal-3* and *hae hsl2 fal-7* and examined the expression of the 67 genes identified in the single-cell/bulk DEG analysis intersection [Supplemental Table 11]. Indeed, in *hae hsl2 fal-3* and *hae hsl2 fal-7,* the majority of these genes show an intermediate level of expression between WT and *hae hsl2* [Figure 5C]. A simple composite way to measure changes in expression of groups of genes is Parametric Analysis of Gene Expression/PAGE, which averages expression of a set of genes on a log scale and uses the resulting approximate normality due to the Central Limit Theorem to perform simple statistical tests[38] (Materials and Methods). Consistent with the hypothesis that the suppressors have partial reversion of the abscission gene expression program, the average log2(FC) levels for both *hae hsl2 fal-3* and *hae hsl2 fal-7* are intermediate between WT and *hae hsl2* [Figure 5D]. These results confirm that pairing scRNA-Seq with bulk analysis can produce validated, efficient transcriptomic characterization useful for acquiring knowledge of molecular pathways.

Mutation of *MAP KINASE PHOSPHATASE-1/MKP1* underlies the *hae hsl2 fal* suppression phenotype

To identify the causative mutations in *fal-3* and *fal-7* we performed complementation crosses, which indicated that *fal-3* and *fal-7* are allelic, recessive mutations [Figure 5E]. To identify the underlying mutations, we performed TAIL-PCR and found *fal-7* harbors a T-DNA insertion in the first exon of *MAP KINASE PHOSPHATASE-1/MKP1,* a gene encoding a phosphatase known to negatively regulate MPK3 and MPK6 during biotic and abiotic stress signaling in a cool-temperature enhanced manner [Figure 5F][39,40]. Because MPK3/6 are also involved in abscission signaling, and because the effect of *fal-3* and *fal-7* is cold-enhanced, *MKP1* became the leading candidate gene. In *fal-3*, we identified a SNP causing a premature stop codon in the first exon of *MKP1* leading to truncation of nearly half the protein [Figure 5F]. In addition, segregation analysis of a back-cross population of *hae hsl2 x hae hsl2 fal-7* indicated the *hae hsl2* suppression effect is linked to the insertion in *MKP1* [Supplementary Figure 6] confirming that the suppression effect of *fal-3* and *fal-7* is due to mutation of *MKP1.*

These results together indicate *MKP1* is a negative regulator of *HAE/HSL2* signaling, allowing us to revise our basic model of abscission signaling [Figure 5G]. In the new model, MKP1 buffers low levels of aberrant signaling, which could otherwise induce abscission in the absence of activation of the *HAE/HSL2* pathway. Thus, MKP1 represents an additional mechanism of regulation that tunes abscission signal strength.

Discussion

This work demonstrates that the abscission zone is transcriptionally distinct as it undergoes rapid differentiation. The gene expression program of the AZ, a consequence of its highly specialized physiology involving middle lamella degradation and cell wall remodeling, renders it especially suitable for single-cell studies due to the ease of cell type identification. Taking advantage of this fact, we have demonstrated the ability to delineate spatially adjacent cell subtypes, the residuum and secession cells of the AZ, each with distinct cellular activities. Our work indicates *HAE/HSL2* signaling promotes the differentiation between these distinct cell types. However, because *HAE* is expressed in both cell types,

specificity factors conferring residuum and secession identity are still unknown. Identification of these factors is a clear target for future research enabled by single-cell technologies.

More generally, we have identified a large number of AZ specific genes and molecular pathways, validating previous results from bulk studies and providing new insights into gene expression and spatial organization of the AZ, pinpointing downstream genes regulated by *HAE HSL2*. Our identification of a negative regulator of abscission, *MKP1,* demonstrates that once single-cell information has been generated and validated, it enables interpretable bulk RNA-Seq analysis as an easier and simpler method to characterize mutants. Testing the activity and regulation of MKP1 during floral organ abscission, and understanding why the suppression effect of *fal-3* and *fal-7* is temperature sensitive, is an exciting direction for future research.

Presumably, the *HAE HSL2* pathway acts by modulating the activity of transcriptional regulators. Future work combining single-cell RNA-Seq with other techniques such as single-cell ATAC-seq and network analysis will help identify cis-regulatory motifs and AZ-expressed transcription factors regulating downstream gene expression programs.

It has been reported that there is substantial genetic variation underlying abscission across the plant kingdom based on differences in the morphology and bulk transcriptome of AZs. Nevertheless, a recent report showed that *Nicotiana* lines with silenced *HAE* and *IDA* orthologs exhibited reduced perianth abscission[41]. In addition, expression of both citrus ad litchi orthologs of *IDA* can complement the abscission-deficient *ida* mutant phenotype in Arabidopsis[42,43]. These results suggests that knowledge of the *HAE/HSL2* pathway will inform regulation of abscission in other dicots. Additionally, we have recently demonstrated abscission of Arabidopsis cauline leaves upon water stress or pathogen infection is under similar genetic control as floral abscission[44,45]. We anticipate application of single-cell RNA-Seq to leaf AZ cells will yield comparably striking information.

Abscission is a key plant behavior with critical relevance to agriculture and the study of domestication. We have uncovered a wealth of biological knowledge about *HAE/HSL2* signaling and expect this work will propel further investigation to identify regulatory mechanisms controlling AZ function.

Methods

Plant growth

The *hae-3 hsl2-3* mutant was used in all experiments[46]. Wild type, *hae-3 hsl2-3, hae-3 hsl2-3 HAEpr::HAE-YFP, hae-3 hsl2-3 HAEpr::HAE-YFP K711E, hae-3 hsl2-3 fal-3,* and *hae-3 hsl2-3 fal-7* are all in the Columbia background. The *fal* suppressor mutants also contain *erecta* and *glabrous* mutations in order to phenotypically differentiate contaminating wild-type seeds from mutants in the *hae hsl2* suppressor screen[24]. Plants were grown in a 16-hour light cycle at either 22° or 16°, except for the breakstrength experiments which were conducted at 23° and 16°. Plants were grown in peat moss/vermiculite potting soil and fertilized every 3 weeks with ½ strength Miracle-Gro (Scotts Miracle-Gro Company).

Protoplasting and FACS

For each protoplast sample, we isolated approximately 20 1 mm sections of stage 15 floral receptacles of plants approximately 2 weeks post-bolting, in a similar manner as our previous work[24,30]. For

protoplasting, we employed the isolation method of Evrard et al, developed for rice roots, with minor modifications[47]. In brief, we prepared digest solution as follows: per 30 mls we added 400 mM mannitol (2.2 g), 20 mM MES hydrate (117 mg), 20 mM KCl (600 µL of 1 M KCl), after which the pH was adjusted to 5.7 with KOH. We would typically make 500 mls of this solution, filter sterilize, and store at 4° for several months. On the day of protoplasting, per 30 mls, we added 1.25% Cellulase R10 (375 mg), 1.25% Cellulase RS (375 mg), 0.3% Macerozyme R10 (90 mg), 0.12% Pectolyase-Y23 (36 mg) and heated 10 min in 60° water bath before cooling to room temperature (all digest enzymes purchased from Duchefa Biochemie except Pectolyase-Y23, which was purchased from MP Biomedicals). Finally we added 10 mM CaCl2 (300 µL of 1 M CaCl2), 0.1% BSA (30 mg), and 5.38 µL of β-mercaptoethanol. We sliced the receptacles into quarters under a dissecting scope on 4% agarose plates with a fine micro-scalpel #715 (Feather), used forceps to transfer into 5 mls of digest solution in small petri dishes, and vacuum infiltrated for 7 minutes at -25 inHg in a dome desiccator. We digested the tissue for 2.25 hours at 80 RPM on a rotary platform shaker at 25°, using fine forceps and micro-scalpel to additionally slice the softened tissue at around 1.5 hours. We next filtered the cells twice through 40 um filters, spun for 5 minutes at 500 x g in a swinging bucket rotor in 5 ml sorting tubes, and rinsed twice with wash buffer (digest buffer with no enzymes). Between washes we spun cells for 3 minutes at 500 x g. Finally, we resuspended cells in wash buffer. It should be noted that it is now recognized calcium in the resuspension buffer reduces the efficiency of reverse transcription[48,49], so it is recommended that for follow-up studies, at least in the final resuspension step, calcium be omitted[49]. For receptacle single-cell samples, cells were counted on a hemacytometer C-chip (SKC, Inc.) and the concentration adjusted to 1000 cells/µl (total yield ranged from approximately 50,000-100,000 cells). For sorted samples, cells were prepared the same manner and sorted for YFP+ on a BD Diva cell-sorter into either excess wash buffer (for single-cell samples) or directly into RNA-Later for bulk samples. Single-cell sorted samples were then spun down and resuspended in 15 µl wash buffer. We took 2.5 µl of cells for dilution and counting on a hemacytometer C-chip. Final yield for sorted samples was between 400-3000 cells, all of which were run on a Chromium chip.

scRNA-Seq library generation

We used the 10x Genomics v3 3' Single-cell RNA-Seq kit for all samples. For the receptacle WT and *hae hsl2* samples we followed the manufacturer's protocol, loading 16,000 cells per sample for a target capture of 10,000 single cells. For sorted samples, we divided a single reaction into four 25 µl reactions and ran on four lanes of a single chip. For sorted sample library preparation, we reduced the volume of all reagents only by ½, which was enabled by excess reagents accumulated due to prior emulsion failures (although we expect miniaturization to ¼-scale library preparations would be feasible). Raw reads have been deposited at the Sequence Read Archive under BioProject PRJNA857332.

scRNA-Seq library sequencing and preprocessing

Unless otherwise noted, all analyses were performed in R 3.6.3 and are included, along with the output of sessionInfo(), as Jupyter Notebooks in the Supplemental Code. We used our previously published scKB procedure to align and produce count matrices for downstream analysis[50]. This pipeline uses kallisto, bustools, busparse, and BSgenome[51–54] to align and quantify counts to the Arabidopsis TAIR10 genome. The following analyses are recorded in Notebook 1: For samples WT and *hae hsl2* receptacle samples #1 we had performed species-mixed experiments containing rice and Arabidopsis cells, so we aligned to a concatenated rice-Arabidopsis MSU7/TAIR10 genome using a combined gff file and retained

only reads mapping to Arabidopsis[50,52]. We pooled reads mapping to spliced and unspliced transcripts in order to make a single matrix of gene expression values. We next ran EmptyDrops[56] in order to identify putative empty droplets containing no cells with "ignore" parameter = 500 and "lower" parameter = 300. We then constructed Seurat objects with the expression matrices. We finally used doubletFinder[57] to identify putative doublets using the approximate doublet rate employed by 10X as .004/500 * # loaded cells. The resulting Seurat objects were used for downstream analysis. Our estimated number of recovered cells after all these steps are: WT receptacle #1: 7509 cells, WT receptacle #2: 7571 cells, WT sorted #1: 878 cells, WT sorted #2: 211 cells, *hae hsl2* receptacle #1: 14492 cells, *hae hsl2* receptacle #2: 7578 cells, *hae hsl2* sorted #1: 1302 cells, *hae hsl2* sorted #2: 1125 cells.

Exploratory analysis of scRNA-Seq data and identification of the AZ

Sample integration (Notebook 2) was performed by running SCTransform on each sample before integrating, excluding mitochondrial genes, plastid genes, and genes altered by protoplasting (defined as those with absolute value of log2(FC) > 1) [Supplemental Table 12]. We performed PCA, constructed a shared nearest neighbor graph, and identified clusters using the SLM algorithm. Visualization was performed by UMAP embedding.

Identification of the AZ (Notebook 3) was performed by first plotting *HAE*, *QRT2*, and *PGAZAT* in WT cells of the UMAP embedding with the "min" parameter set to .5. We next calculated the pseudobulk expression profile for all clusters identified at resolution .75 by summing all counts for each gene. We next calculated Spearman correlation with bulk sorted *HAE+* and *QRT2+* RNA-Seq data. The *HAE* data (Supplemental Table 1) was Lexogen Quant-seq 3' and consequently is directly convertible to Transcripts per Million (TPM) making it comparable to 3' RNA-Seq data generated by Chromium 10X. Because the *QRT2* data (Supplemental Table 2) include separate secession and residuum derived cells, we first created an approximate composite AZ transcriptome by summing the counts per million for both secession and residuum datasets with equal weighting. This dataset was full-transcript RNA-Seq, so we estimated TPM using the formula below (Supplemental Table 3):

$$TPM_{geneX} = \frac{\frac{count_{geneX}}{length_{geneX}}}{\Sigma\left(\frac{count_{each_{gene}}}{length_{each_{gene}}}\right)} * 1{,}000{,}000$$

We then plotted the correlation value for each cluster on the previously generated UMAP embedding.

Promoter cloning

Fragments ranging in size from 1 to 2.5 kilobases upstream of *MYB62*, *PECTIN LYASE-LIKE*, and *GDSL-TYPE ESTERASE* were PCR amplified with PfuUltraII polymerase and cloned into pENTR (ThermoFisher), then recombined into pMDC111[58] to create promoter::GFP fusions (primers are listed in Supplemental Table 13). The *FAR5* upstream region was PCR amplified by KAPA Hifi polymerase (Roche) and cloned into an *Oryza sativa* H2B-VENUS fusion construct created by gene synthesis (Twist Bioscience). The *H2B-VENUS* construct was first cloned into pENTR and recombined into pGWB501[59]. This construct was created to include two AarI sites for Golden Gate cloning of promoter fragments in one step. Primers are included in Supplemental Table 13. Siliques were imaged on a Zeiss Axiozoom stereomicroscope with UV illumination.

Non-Abscission zone Cell Annotation

Clusters were defined by twice running the Seurat FindClusters function with both a low modularity parameter (res = 2) and a high modularity parameter (res = 200), which results in clusters containing hundreds/thousands of cells (broadly-resolved) and those having only tens of cells each (finely-resolved), respectively. We then calculated expression z-scores of known marker genes [Supplemental Table 14] in each cluster (both broadly and finely-resolved). These clusters were then annotated by comparing the average marker gene z-scores. Cells that were annotated with the same cell identity in broadly-resolved and finely-resolved clusters were considered confidently annotated. While those that were not were labeled as "Unknown." This annotation approach combining results of complementary modularity resolution was particularly useful for annotating rare cell-types while maintaining low noise levels (Notebook 4).

AZ pseudo-bulk DEG analysis comparing WT and *hae hsl2*

We performed pseudo-bulking for the AZ (Seurat cluster 11) for each WT and *hae hsl2* sample, yielding four samples for each genotype (Notebook 5). We then used edgeR to normalize and calculate CPM and LCPM matrices. We modeled whether the cells were sorted as a nuisance factor (to account for variation due to FACS), and otherwise only included genotype as a factor (WT or mutant). We then constructed a contrast testing the hypothesis that the genotype factor for the difference in expression between WT and *hae hsl2* for each gene was equal to 0. The output of edgeR has been included as Supplemental Table 6. A file with our edgeR functions has been included in Supplemental Code. This code requires an Arabidopsis annotation file derived from TAIR10 included as Supplemental Table 15.

GO term analysis

For GO analysis we used shinyGO v 0.76[60]. For all analyses we displayed Biological Process terms at FDR < .01. For GO analysis of WT AZs we used the output of the Seurat FindAllMarkers function to select genes log2(Fold Enrichment) > 1 with FDR < .05 in the AZ. We used all genes from the FindAllMarkers analysis as a universe (IE, genes expressed in at least one cluster). For the WT-mutant DE GO analysis, we took genes defined as DE log2(FC) > 1 with FDR < .05 with all genes expressed in at least 3 samples as universe. GO analysis of the bulk DE/single-cell DE intersection was performed with a universe as the genes defined to be expressed in the WT/*hae hsl2* pseudo-bulk DEG analysis.

AZ subclustering

AZ cells (those from cluster 11) were sub-divided into those of WT and *hae hsl2* origin, and each dataset was reintegrated using a similar process as above (Notebook 6). We then performed coarse clustering with resolution = .1 in Seurat which identified two transcriptionally distinct groups for both genotypes. We performed pseudo-bulk Spearman correlation analysis comparing expression of each of the two clusters in each genotype to previously published FACS secession and residuum datasets[15]. For enrichment analysis we took the pseudo-bulked putative residuum cells and secession cells and performed edgeR analysis as above, except we pooled the cells derived from the two FACS samples for both mutant and WT due to a particularly low number of cells in WT sorted sample #1. The secession and residuum associated genes are those with FDR < .05 and log2(fold enrichment) > 1 in the respective cell types. We will note because the cells were clustered first before running the edgeR analysis, the resulting gene lists were not unbiased estimates of differential expression. However, because we

441 performed identical procedures for WT and mutant and our Fisher's exact test is testing the hypothesis
442 that the proportion of genes in this "enriched" set is different between the two genotypes.

443 **Bulk RNA-Seq library generation and sequencing**

444 For the sorted *HAE-YFP* bulk samples, we sorted into 20 µl of RNA-Later then used the magnetic bead
445 based Direct-zol-96 MagBead RNA-Isolation kit (Zymo) to isolate RNA. For the protoplast test, we cut
446 three receptacles per replicate and digested as above. We harvested the tissue by spinning at 500 x g
447 and removing supernatant, leaving digested cells and undigested tissue in place, before freezing in liquid
448 N2. We simultaneously collected three receptacles per replicate in our unprotoplasted control where
449 tissue was placed in 10 µl of RNA-Later in the cap of a 1.7 ml microcentrifuge tube, tapped to the
450 bottom of the tube, immediately frozen in liquid N2, homogenized with a blue pestle, and performed
451 RNA isolation as above. We performed three replicates in each condition.

452 For the *fal-3/fal-7* bulk RNA-Seq experiment, we isolated receptacles from three stage 15 flowers for
453 each replicate of *er gl* (WT grandparent), *er gl hae-3 hsl2-3* (mutant parent), and *er gl hae-3 hsl2-3 fal-*
454 *3/fal-7* (suppressors). Tissue was placed into the cap of a 1.7 ml tube containing 10 µl RNA-Later. After
455 tapping the tissue to the bottom of the tube, we froze in liquid nitrogen. We then ground the tissue in
456 liquid N2 using blue pestles, and used the Zymo RNA-isolation kit as before. For all samples, RNA
457 integrity was checked with Bioanalyzer RNA Nano kit and quantified by Qubit.

458 For library generation, we used Lexogen Quantseq RNA-Seq using the manufacturer's protocol, with
459 instructions for "Low input" for the sorted samples due to input of only 5-10 ng total RNA input per
460 sample. We used the Unique Molecular Identifier (UMI) PCR add-on kit (Lexogen). Libraries were
461 indexed and sequenced on an Illumina NextSeq, High Output setting. Reads were aligned to the TAIR10
462 genome using the STAR aligner, deduplicated using UMI-Tools, and counted with HTSeq-Count. Counts
463 were analyzed with edgeR. We defined "expressed genes" to be those with observed reads in three or
464 more libraries. Raw reads have been deposited at the Sequence Read Archive under BioProject
465 PRJNA857332.

466 **PAGE analysis of abscission-associated gene expression in *fal* mutants**

467 We constructed an expression matrix for the 67 bulk/single-cell intersection gene set for WT, *hae hsl2,*
468 *hae hsl2 fal-3,* and *hae hsl2 fal-3* using the log2(CPM) values generated by edgeR (Notebooks 7 and 8).
469 We then summed the log2(CPM) values of each gene for each sample and normalized to the average
470 summed values of the *hae hsl2* samples before dividing by the number of genes in the analysis. The
471 resulting quantity represents the average log2(FC) for each sample compared to the *hae hsl2* average.
472 Last, we performed pairwise T-tests with Bonferroni Correction assuming equal variance.

473 **Breakstrength measurements**

474 The breakstrength of petals of stage 16 flowers (ie, silique 1-2 mm above petals) in *er gl hae-3 hsl2-3*
475 and *er gl hae-3 hsl2-3 fal-3/7* were measured using our previously described petal break strength meter
476 and analysis script[61]. In brief, the petals were clamped to the meter and the flower pulled down with
477 forceps until the petal detached. The maximum voltage was extracted from the output file of the meter.
478 This voltage reading was converted to an equivalent force after calculation of a standard curve based on
479 voltage readings of the meter attached to a varying number of objects of known weight (ie, paper clips).

For measurements taken at each temperature, we performed pairwise T-tests with Bonferroni Correction assuming equal variance.

fal mutant identification

The *hae-3 hsl2-3* suppressor screen was performed as previously described[24]. For identification, we used TAIL-PCR[62] to amplify a PCR fragment in *fal-7* which was analyzed by Sanger sequencing. For *fal-3,* we used TAIL-PCR to identify an insertion in an exon of AT2G07690, which is a member of the Minichromosome Maintenance gene family involved in initiation of DNA replication. However, given the similar phenotype of *fal-7* we hypothesized there may exist an additional mutation in *MKP1*. We designed Sanger sequencing primers and tiled the coding sequence, detecting a G-> A SNP at bp 1357 in the *MKP1* coding sequence using primers listed in Supplemental Table 13. We performed linkage analysis in the *hae hsl2 x hae hsl2 fal-7* F2 population using genotyping primers listed in Supplemental Table 13.

Conflict of Interest

The authors declare they have no conflict of interest.

Funding

This work was supported by NSF MCB0743955 to JCW, NIH 1R35GM131725 to PNB, who is also supported by the Howard Hughes Medical Institute as an investigator, USDA 2021-67034-35139 to IWT, and Deutsche Forschungsgemeinschaft (DFG) 2403 to UO and CWH.

1. Addicott, F. T. & Lynch, R. S. Physiology of abscission. *Annual Review of Plant Physiology* **6**, 211–238 (1955).
2. Taylor, J. E. & Whitelaw, C. A. Signals in abscission. *New Phytologist* **151**, 323–340 (2001).
3. Patharkar, O. R. & Walker, J. C. Connections between abscission, dehiscence, pathogen defense, drought tolerance, and senescence. *Plant Science* **284**, 25–29 (2019).
4. Yu, Y. & Kellogg, E. A. Inflorescence abscission zones in grasses: diversity and genetic regulation. *Annual Plant Reviews* **1**, 1–35 (2018).
5. Dutta, S. K., Gurung, G., Yadav, A., Laha, R. & Mishra, V. K. Factors associated with citrus fruit abscission and management strategies developed so far: A review. *New Zealand Journal of Crop and Horticultural Science* 1–22 (2022).
6. Kaur, R., Deol, J. & Dass, A. Physiology of abscission and crop regulation in cotton-a review. (2016).

7. Hossain, S., Kadkol, G., Raman, R., Salisbury, P. & Raman, H. Breeding Brassica napus for shatter resistance. *In Plant Breeding* (2011).

8. Li, L.-F. & Olsen, K. To have and to hold: selection for seed and fruit retention during crop domestication. *Current topics in developmental biology* **119**, 63–109 (2016).

9. Tranbarger, T. J. & Tadeo, F. R. Diversity and functional dynamics of fleshy fruit abscission zones. *Annual Plant Reviews online* 1–64 (2018).

10. Patharkar, O. R. & Walker, J. C. Advances in abscission signaling. *J Exp Bot* **69**, 733–740 (2018).

11. Meir, S. *et al.* Re-evaluation of the ethylene-dependent and-independent pathways in the regulation of floral and organ abscission. *Journal of experimental botany* **70**, 1461–1467 (2019).

12. Ellis, C. M. *et al.* AUXIN RESPONSE FACTOR1 and AUXIN RESPONSE FACTOR2 regulate senescence and floral organ abscission in Arabidopsis thaliana. *Development* **132**, 4563–4574 (2005).

13. Basu, M. M. *et al.* The manipulation of auxin in the abscission zone cells of Arabidopsis flowers reveals that indoleacetic acid signaling is a prerequisite for organ shedding. *Plant physiology* **162**, 96–106 (2013).

14. Kim, J. *et al.* New clothes for the jasmonic acid receptor COI1: delayed abscission, meristem arrest and apical dominance. *PloS one* **8**, e60505 (2013).

15. Lee, Y. *et al.* A lignin molecular brace controls precision processing of cell walls critical for surface integrity in Arabidopsis. *Cell* **173**, 1468–1480 (2018).

16. Patterson, S. E. Cutting Loose. Abscission and Dehiscence in Arabidopsis. *Plant Physiology* **126**, 494–500 (2001).

17. Jinn, T. L., Stone, J. M. & Walker, J. C. HAESA, an Arabidopsis leucine-rich repeat receptor kinase, controls floral organ abscission. *Genes Dev.* **14**, 108–117 (2000).

18. Cho, S. K. *et al.* Regulation of floral organ abscission in Arabidopsis thaliana. *Proc. Natl. Acad. Sci. U.S.A.* **105**, 15629–15634 (2008).

19. Stenvik, G.-E. *et al.* The EPIP peptide of INFLORESCENCE DEFICIENT IN ABSCISSION is sufficient to induce abscission in arabidopsis through the receptor-like kinases HAESA and HAESA-LIKE2. *Plant Cell* **20**, 1805–1817 (2008).

20. Patharkar, O. R. & Walker, J. C. Floral organ abscission is regulated by a positive feedback loop. *Proceedings of the National Academy of Sciences* 201423595 (2015).

21. Butenko, M. A. *et al.* INFLORESCENCE DEFICIENT IN ABSCISSION controls floral organ abscission in Arabidopsis and identifies a novel family of putative ligands in plants. *The Plant Cell Online* **15**, 2296–2307 (2003).

22. Santiago, J. *et al.* Mechanistic insight into a peptide hormone signaling complex mediating floral organ abscission. *Elife* **5**, e15075 (2016).

23. Meng, X. *et al.* Ligand-induced receptor-like kinase complex regulates floral organ abscission in Arabidopsis. *Cell reports* **14**, 1330–1338 (2016).

24. Taylor, I., Baer, J., Calcutt, R. & Walker, J. C. Hypermorphic SERK1 mutations function via a SOBIR1 pathway to activate floral abscission signaling. *Plant physiology* **180**, 1219–1229 (2019).

25. Niederhuth, C. E., Patharkar, O. R. & Walker, J. C. Transcriptional profiling of the Arabidopsis abscission mutant hae hsl2 by RNA-Seq. *BMC Genomics* **14**, 37 (2013).

26. Butenko, M. A. *et al.* Ethylene-dependent and -independent pathways controlling floral abscission are revealed to converge using promoter::reporter gene constructs in the ida abscission mutant. *J. Exp. Bot.* **57**, 3627–3637 (2006).

27. Müller, A. Zur Charakterisierung der Blüten und Infloreszenzen vonArabidopsis thaliana (L.) Heynh. *Die Kulturpflanze* **9**, 364–393 (1961).

28. Smyth, D. R., Bowman, J. L. & Meyerowitz, E. M. Early flower development in Arabidopsis. *The Plant Cell* **2**, 755–767 (1990).

29. Taylor, I. *et al.* Analysis of Phosphorylation of the Receptor-Like Protein Kinase HAESA during Arabidopsis Floral Abscission. *PLoS ONE* **11**, e0147203 (2016).

30. Taylor, I. & Walker, J. C. Transcriptomic evidence for distinct mechanisms underlying abscission deficiency in the Arabidopsis mutants haesa/haesa-like 2 and nevershed. *BMC Research Notes* **11**, 754 (2018).

31. Cai, S. & Lashbrook, C. C. Stamen abscission zone transcriptome profiling reveals new candidates for abscission control: enhanced retention of floral organs in transgenic plants overexpressing Arabidopsis ZINC FINGER PROTEIN2. *Plant physiology* **146**, 1305–1321 (2008).

32. Stuart, T. *et al.* Comprehensive integration of single-cell data. *Cell* **177**, 1888–1902 (2019).

33. Zhang, T.-Q., Chen, Y. & Wang, J.-W. A single-cell analysis of the Arabidopsis vegetative shoot apex. *Developmental Cell* **56**, 1056–1074 (2021).

34. Klepikova, A. V., Kasianov, A. S., Gerasimov, E. S., Logacheva, M. D. & Penin, A. A. A high resolution map of the Arabidopsis thaliana developmental transcriptome based on RNA-seq profiling. *The Plant Journal* **88**, 1058–1070 (2016).

35. Zhou, Y. *et al.* Genetic control of seed shattering in rice by the APETALA2 transcription factor SHATTERING ABORTION1. *The Plant Cell* **24**, 1034–1048 (2012).

36. Robinson, M. D., McCarthy, D. J. & Smyth, G. K. edgeR: a Bioconductor package for differential expression analysis of digital gene expression data. *Bioinformatics* **26**, 139–140 (2010).

37. Sexton, R. & Roberts, J. A. Cell biology of abscission. *Annual Review of Plant Physiology* **33**, 133–162 (1982).

38. Kim, S.-Y. & Volsky, D. J. PAGE: Parametric Analysis of Gene Set Enrichment. *BMC Bioinformatics* **6**, 144 (2005).

39. Ulm, R. *et al.* Distinct regulation of salinity and genotoxic stress responses by Arabidopsis MAP kinase phosphatase 1. *The EMBO Journal* **21**, 6483–6493 (2002).

580 40. Bartels, S. *et al.* MAP kinase phosphatase1 and protein tyrosine phosphatase1 are repressors of
581 salicylic acid synthesis and SNC1-mediated responses in Arabidopsis. *The Plant Cell* **21**, 2884–2897
582 (2009).
583 41. Ventimilla, D. *et al.* IDA (INFLORESCENCE DEFICIENT IN ABSCISSION)-like peptides and HAE
584 (HAESA)-like receptors regulate corolla abscission in Nicotiana benthamiana flowers. *BMC plant*
585 *biology* **21**, 1–14 (2021).
586 42. Estornell, L. H. *et al.* The IDA peptide controls abscission in Arabidopsis and Citrus. *Frontiers in*
587 *plant science* **6**, 1003 (2015).
588 43. Ying, P. *et al.* Identification and molecular characterization of an IDA-like gene from litchi,
589 LcIDL1, whose ectopic expression promotes floral organ abscission in Arabidopsis. *Scientific Reports*
590 **6**, 1–11 (2016).
591 44. Patharkar, O. R. & Walker, J. C. Core Mechanisms Regulating Developmentally Timed and
592 Environmentally Triggered Abscission. *Plant Physiol.* **172**, 510–520 (2016).
593 45. Patharkar, O. R., Gassmann, W. & Walker, J. C. Leaf shedding as an anti-bacterial defense in
594 Arabidopsis cauline leaves. *PLoS genetics* **13**, e1007132 (2017).
595 46. Niederhuth, C. E., Cho, S. K., Seitz, K. & Walker, J. C. Letting Go is Never Easy: Abscission and
596 Receptor-Like Protein Kinases. *Journal of integrative plant biology* **55**, 1251–1263 (2013).
597 47. Evrard, A. *et al.* Fluorescence-activated cell sorting for analysis of cell type-specific responses to
598 salinity stress in Arabidopsis and rice. in *Plant Salt Tolerance* 265–276 (Springer, 2012).
599 48. Tan, C. K. *et al.* Functional characterization of RNA-dependent DNA polymerase and RNase H
600 activities of a recombinant HIV reverse transcriptase. *Biochemistry* **30**, 2651–2655 (1991).
601 49. Denyer, T. & Timmermans, M. C. Crafting a blueprint for single-cell RNA sequencing. *Trends in*
602 *Plant Science* (2021).

603 50. Shahan, R. *et al.* A single-cell Arabidopsis root atlas reveals developmental trajectories in wild-
604 type and cell identity mutants. *Developmental cell* **57**, 543–560 (2022).
605 51. Bray, N. L., Pimentel, H., Melsted, P. & Pachter, L. Near-optimal probabilistic RNA-seq
606 quantification. *Nature biotechnology* **34**, 525–527 (2016).
607 52. Melsted, P., Ntranos, V. & Pachter, L. The barcode, UMI, set format and BUStools. *Bioinformatics*
608 **35**, 4472–4473 (2019).
609 53. Moses, L. & Pachter, L. BUSpaRse: kallisto| bustools R utilities. *R package version* **1**, (2019).
610 54. Pagès, H. BSgenome: Software infrastructure for efficient representation of full genomes and
611 their SNPs. *R package version 1.64.0, https://bioconductor.org/packages/BSgenome* (2020).
612 55. Kawahara, Y. *et al.* Improvement of the Oryza sativa Nipponbare reference genome using next
613 generation sequence and optical map data. *Rice* **6**, 1–10 (2013).
614 56. Lun, A. T., Riesenfeld, S., Andrews, T., Gomes, T. & Marioni, J. C. EmptyDrops: distinguishing cells
615 from empty droplets in droplet-based single-cell RNA sequencing data. *Genome biology* **20**, 1–9
616 (2019).
617 57. McGinnis, C. S., Murrow, L. M. & Gartner, Z. J. DoubletFinder: doublet detection in single-cell
618 RNA sequencing data using artificial nearest neighbors. *Cell systems* **8**, 329–337 (2019).
619 58. Curtis, M. D. & Grossniklaus, U. A gateway cloning vector set for high-throughput functional
620 analysis of genes in planta. *Plant physiology* **133**, 462–469 (2003).
621 59. Nakagawa, T. *et al.* Development of series of gateway binary vectors, pGWBs, for realizing
622 efficient construction of fusion genes for plant transformation. *Journal of bioscience and*
623 *bioengineering* **104**, 34–41 (2007).
624 60. Ge, S. X., Jung, D. & Yao, R. ShinyGO: a graphical gene-set enrichment tool for animals and
625 plants. *Bioinformatics* **36**, 2628–2629 (2020).

61. Lease, K. A., Cho, S. K. & Walker, J. C. A petal breakstrength meter for Arabidopsis abscission studies. *Plant Methods* **2**, 2 (2006).

62. Liu, Y.-G., Mitsukawa, N., Oosumi, T. & Whittier, R. F. Efficient isolation and mapping of Arabidopsis thaliana T-DNA insert junctions by thermal asymmetric interlaced PCR. *The Plant Journal* **8**, 457–463 (1995).

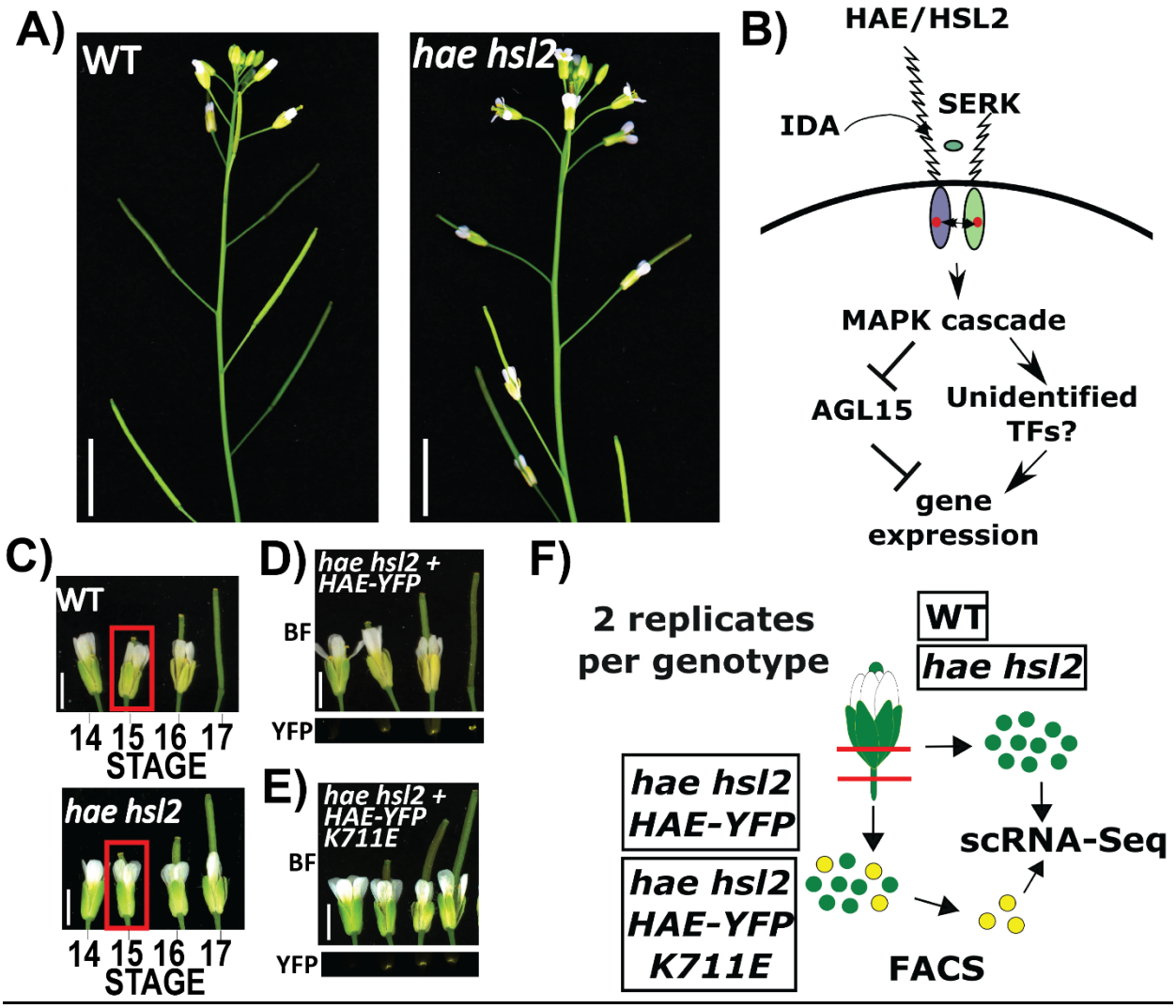

Figure 1: Background and experimental system

A) Floral abscission phenotype of WT and *hae hsl2* mutant. Scale bar = 10 mm.
B) Schematic diagram of HAE/HSL2 signaling pathway.
C) Flower stages in WT and *hae hsl2* mutant. Scale bar = 2 mm.
D) Phenotype of transgenic *hae hsl2* expressing wild-type *HAEpr::HAE-YFP* (top: bright-field/BF, lower: YFP). Scale bar = 2 mm.
E) Phenotype of transgenic *hae* hsl2 expressing mutant *HAEpr::HAE-YFP K711E* (top: bright-field/BF, lower: YFP). Scale bar = 2 mm.
F) Diagram of AZ single-cell isolation and experimental procedure.

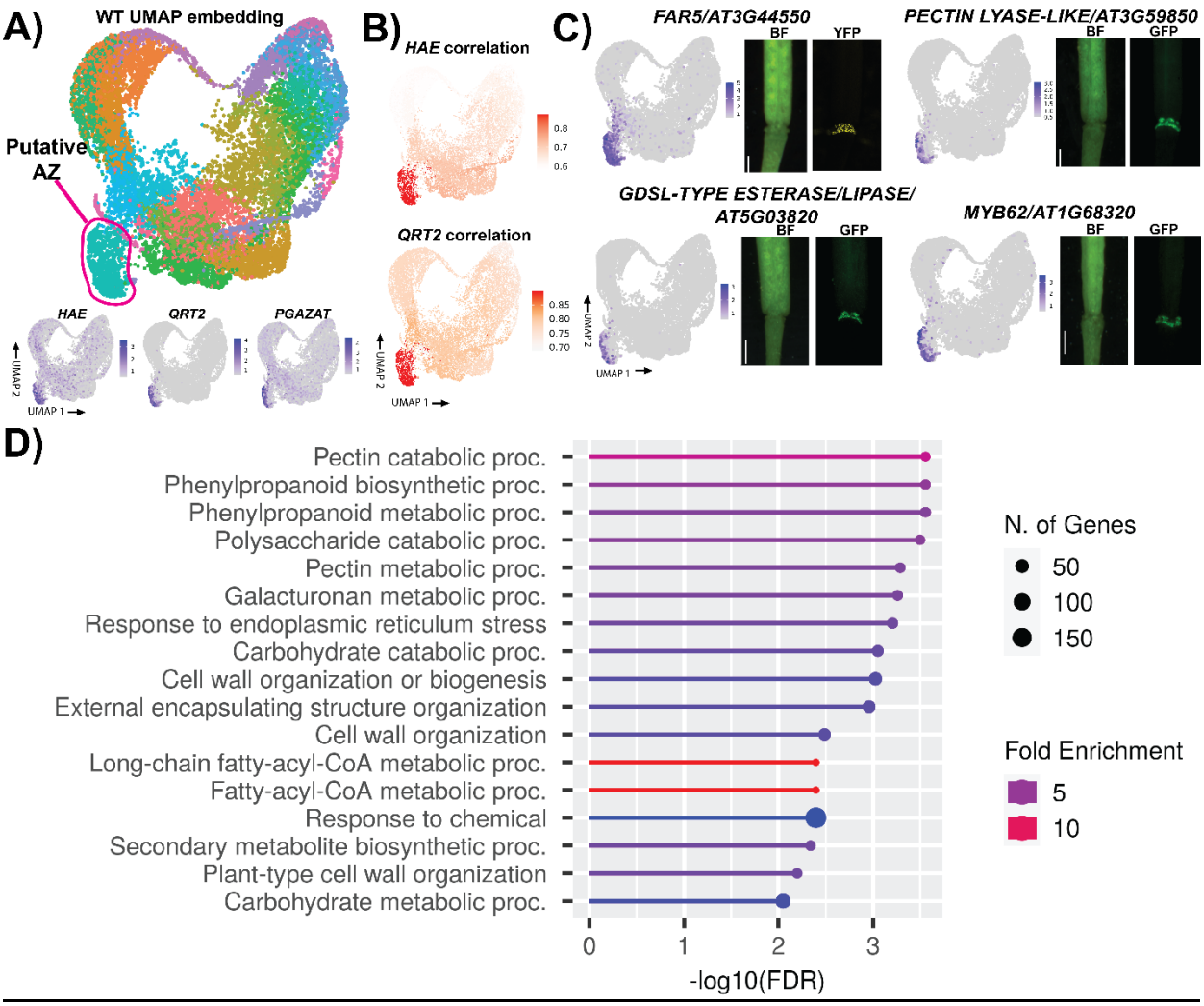

Figure 2: Identification and characterization of AZ cells by single-cell RNA-Sequencing

A) UMAP embedding of WT cells with putative AZ cluster circles in pink (top) and expression of AZ marker genes on UMAP (bottom). Expression is on Seurat SCT scale.

B) Cluster-wise pseudo-bulk Spearman correlation with sorted bulk data of *HAEpr::HAE-YFP* (top) or *QRT2pr::GFP* (bottom).

C) Expression of 4 putative AZ marker genes in single-cell UMAP embedding and in the young siliques of *promoter::fluorescent protein* expressing transgenic plants (bright-field/BF and YFP or GFP). Expression is on Seurat SCT scale. Scale bar = .7 mm.

D) Gene Ontology Biological Process term enrichment of AZ specific genes.

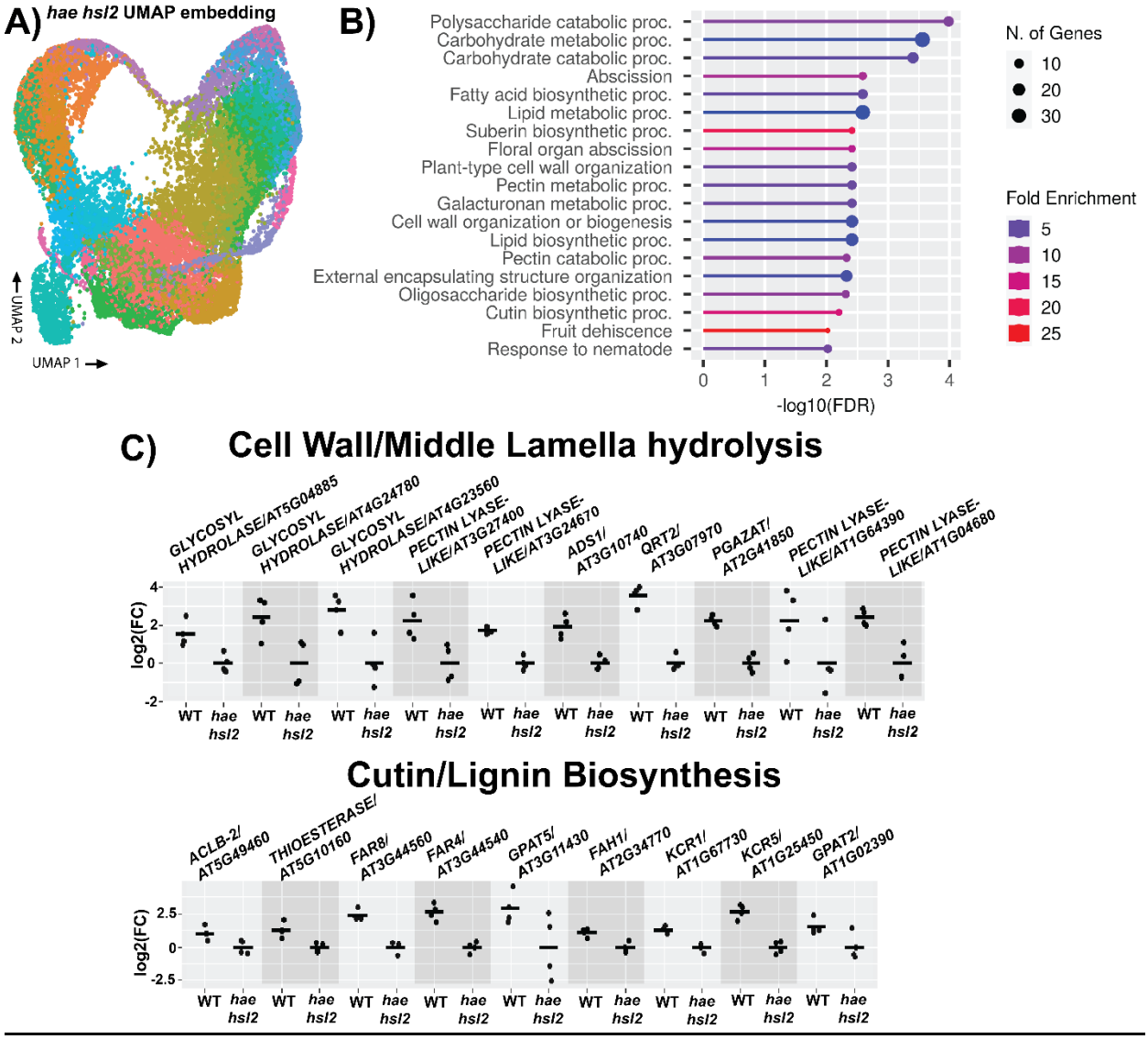

Figure 3: Analysis of differentially expressed genes in the *hae hsl2* mutant AZ

A) UMAP embedding of *hae hsl2* cells.

B) Gene Ontology Biological Process term enrichment of DE genes higher in WT (FDR <.05, log2(FC) > 1).

C) Expression of cell wall/middle lamella hydrolysis genes (top) and cutin/lignin biosynthesis genes (bottom). Scale is log2(FC) for each sample relative to the average of *hae hsl2*.

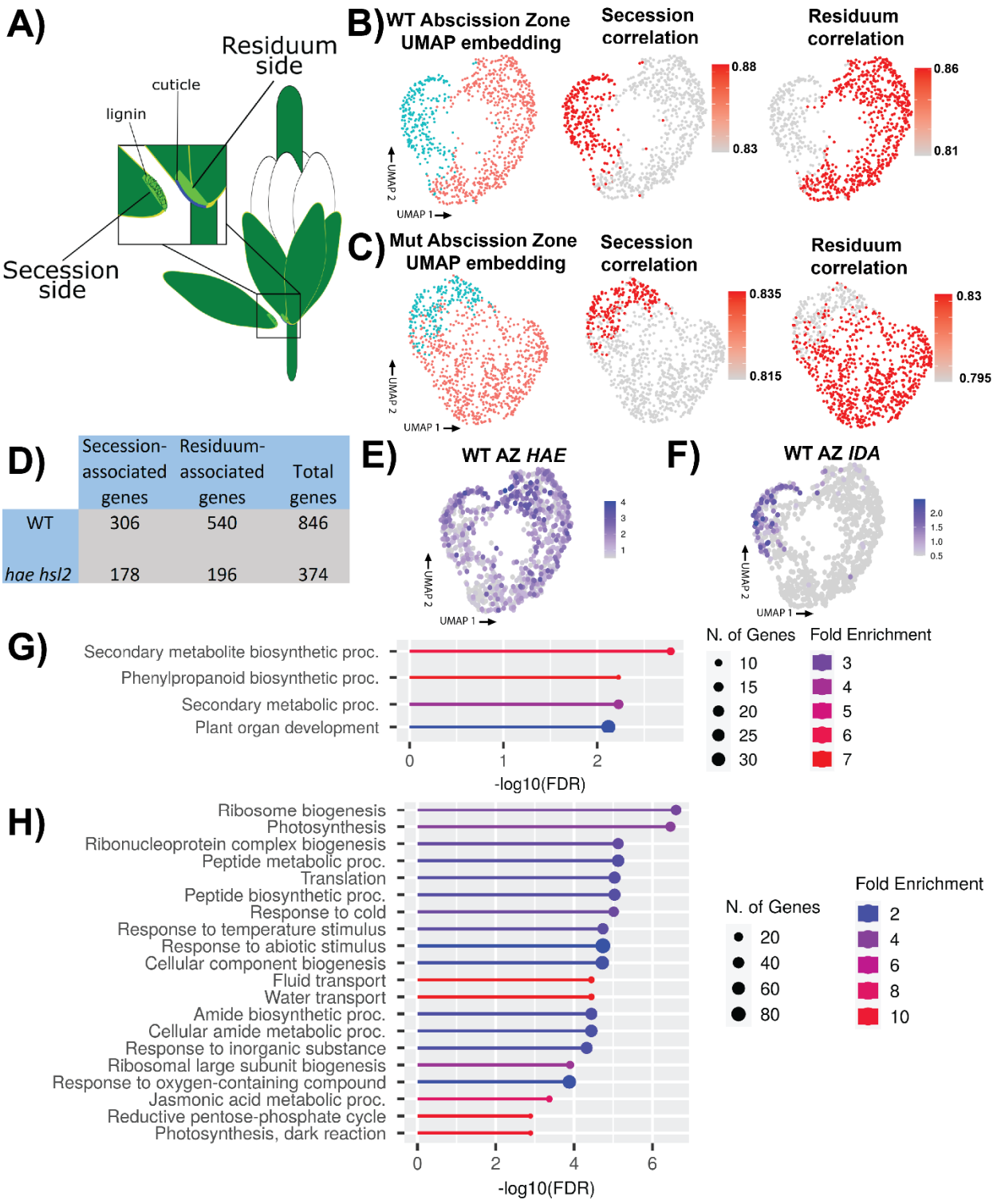

Figure 4: Spatial analysis of the AZ

A) Schematic view of the spatial organization of the AZ.

B) Low resolution Louvain clustering and UMAP embedding of WT AZ cells (left) and Spearman correlation with sorted bulk secession data (middle) or residuum data (right).

C) Low resolution Louvain clustering and UMAP embedding of *hae hsl2* AZ cells (left) and Spearman correlation with sorted bulk secession data (middle) or residuum data (right).
D) Tabulation of differences in the number of secession and residuum-associated genes between WT and *hae hsl2*.
E) Expression of *HAE* on SCT scale across the AZ.
F) Expression of *IDA* on SCT scale across the AZ.
G) Gene Ontology Biological Process term enrichment of genes enriched in putative secession cells.
H) Gene Ontology Biological Process term enrichment of genes enriched in putative residuum cells.

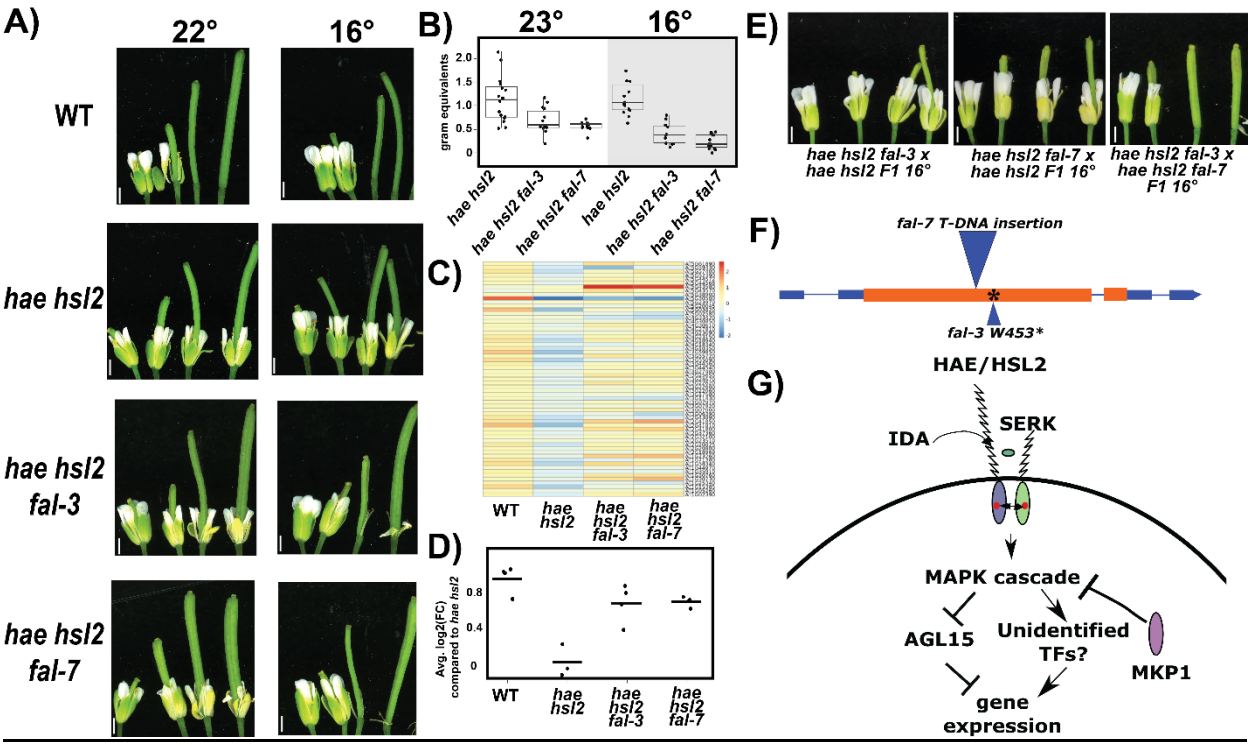

Figure 5: Analysis and identification of *hae hsl2* suppressors

A) Phenotypes of WT, *hae hsl2, hae hsl2 fal-3,* and *hae hsl2 fal-7* at 22° (left) or 16° (right). Siliques were gently tapped to remove remnant floral organs. Scale bar = 1 mm.

B) Breakstrength phenotypes of *hae hsl2, hae hsl2 fal-3,* and *hae hsl2 fal-7* at 23° (left) or 16° (right).

C) Heatmap of expression values for 67 genes identified as higher in WT in both bulk and single-cell DE analysis comparing WT to *hae hsl2.* Values are log2(FC) compared the overall average expression across all genotypes.

D) Average log2(FC) comparing each sample to the average of *hae hsl2* for the genes in part C.

E) Complementation crosses of *fal* mutants. Scale bar = 1 mm.

F) Gene model of *MKP1* depicting mutations in *fal-3* and *fal-7.* Orange colors represent exons, blue represent UTRs, and thin lines represent introns.

G) Revised schematic diagram of HAE/HSL2 signaling pathway

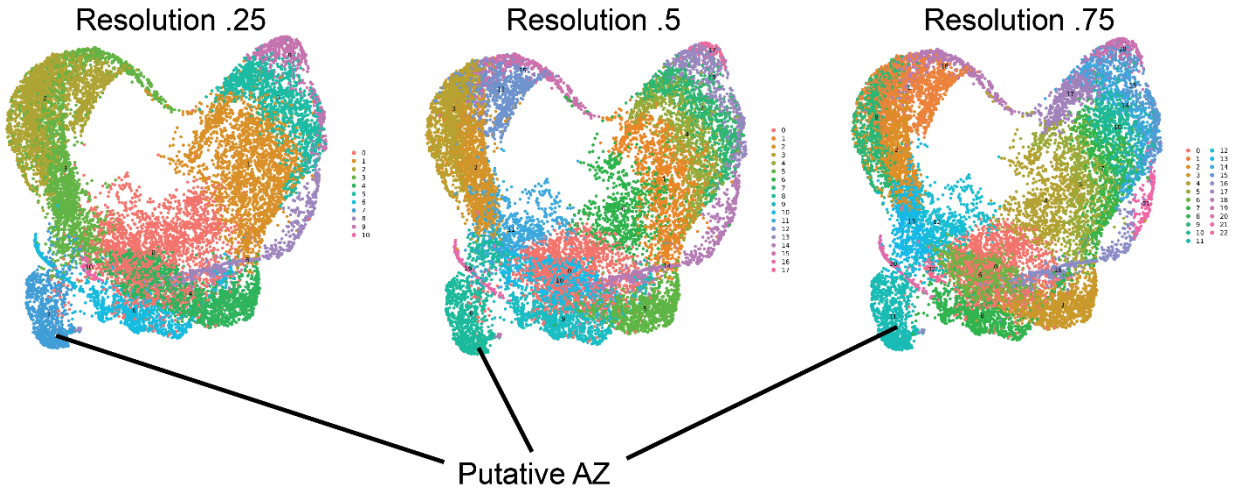

Supplemental Figure 1: The putative AZ cluster is similar across a range of clustering resolutions

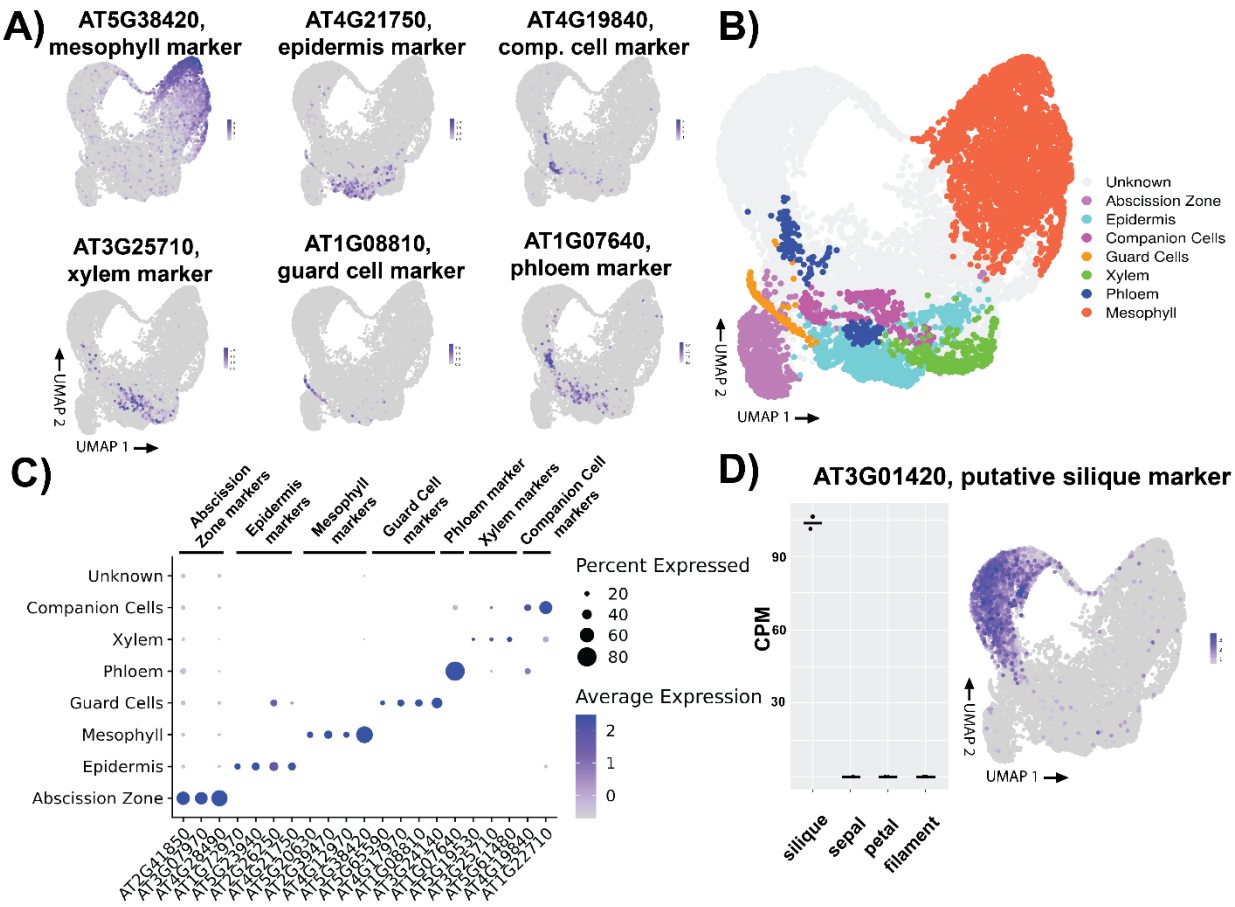

<u>Supplemental Figure 2</u>: Identification of additional cell types

A) Plotting cell type markers identified from a prior single-cell study of Arabidopsis leaves.
B) Tentative cell-type identification based on expression of known marker cell-type marker genes.
C) Distribution of marker gene expression across putative cell types.
D) Expression of putative silique marker gene in previously published bulk data (left panel), and expression of the same putative silique marker gene from our single-cell data (right panel).

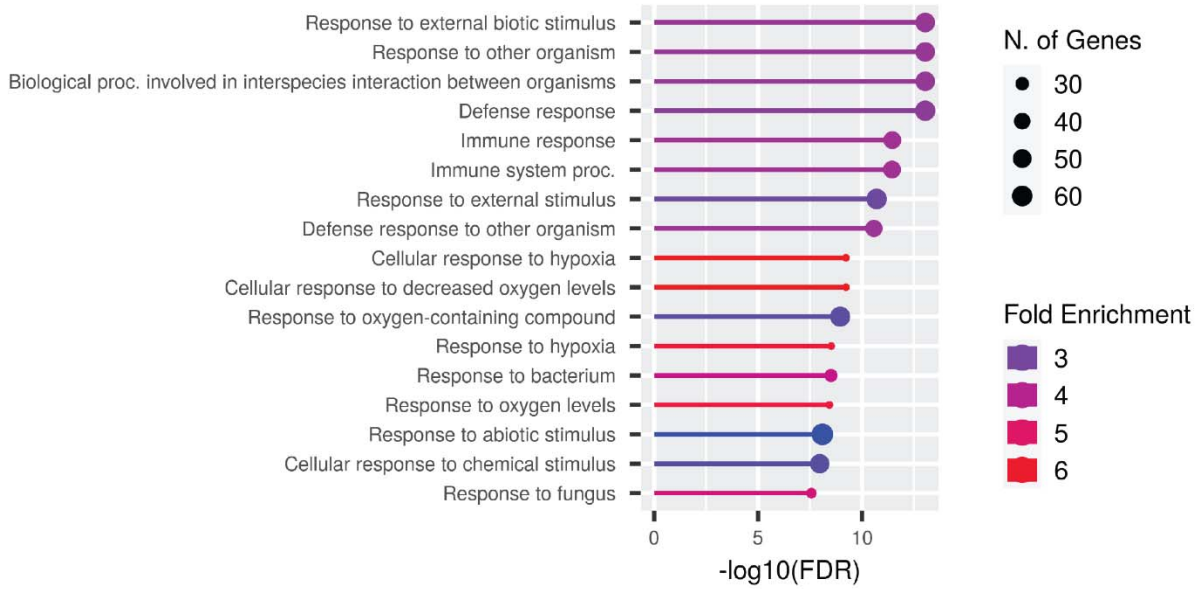

<u>Supplemental Figure 3:</u> GO term enrichment analysis of genes higher in *hae hsl2* compared to WT AZs.

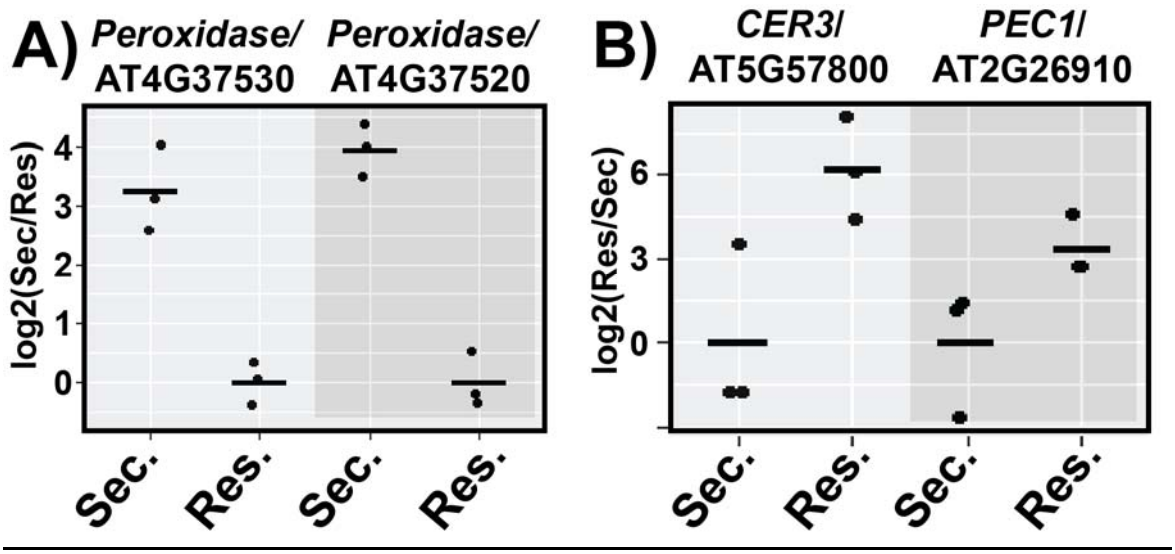

Supplemental Figure 4: Expression of putative secession and residuum cell markers

A) Relative log2(fold enrichment) of two peroxidase genes in secession cells.
B) Relative log2(fold enrichment) of two cutin biosynthesis genes in residuum cells.

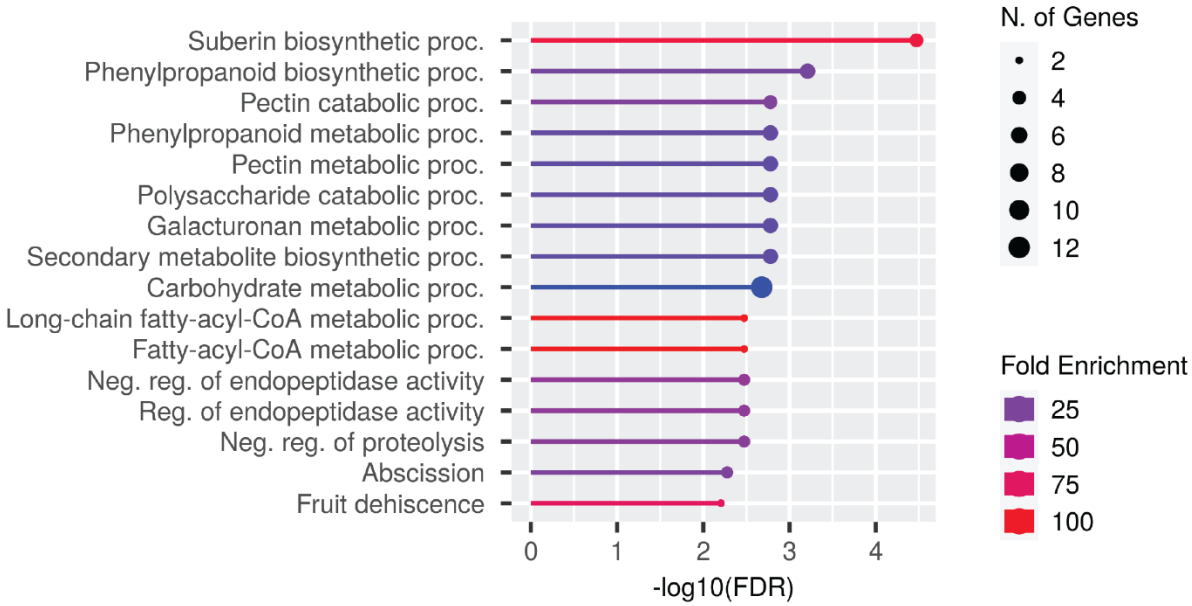

<u>Supplemental Figure 5:</u> GO term enrichment analysis of genes lower in *hae hsl2* compared to WT from both bulk and single-cell RNA-Seq.

genotype	+/+	+/*fal-7*	*fal-7*/*fal-7*
suppression phenotype	0/8	0/34	18/18

Supplemental Figure 6: Association of phenotype and genotype in an F2 *hae hsl2 x hae hsl2 fal-7* backcross population.